

Size-dependent optical imaging properties of high-index immersed microsphere lens

Minglei Guo^{1,2} · Yong-Hong Ye¹ · Jinglei Hou¹ · Bintao Du¹

Received: 16 July 2015 / Accepted: 16 January 2016 / Published online: 12 March 2016
© Springer-Verlag Berlin Heidelberg 2016

Abstract The imaging properties of high-index immersed microsphere lenses in the diameter range of 5–300 μm are experimentally studied. Our experimental results show that shifting the focal plane of the objective lens can result in different optical properties. When light beams generated from the objective lens are focused near the low surface of the microsphere lens, interference rings can be observed by a conventional optical microscopy, and its diameter and ring number increase with the diameter of microspheres, which can be similarly described by conventional wave optics. When the focal plane of the objective lens is further turned down about several microns, the Blu-ray disk with sub-wavelength structures can be discerned with a magnification up to $4.5\times$ and field of view up to 14 μm . The image contrast and resolution decrease as the microsphere diameter increases. Calculations of the electric field distributions indicate that the “photonic nanojet” induced by the microsphere performs an important role in sub-wavelength imaging. The surrounding medium can be expected to improve the formation of both the sub-wavelength images and the interference rings. Our studies will help the understanding of the imaging mechanisms in microsphere lenses.

1 Introduction

Motivated by beating Abbe’s diffraction limit, scientists have proposed many approaches to realize super-resolution imaging. These techniques include negative index metamaterials [1, 2], fluorescence microscopy [3], near-field scanning [4], hyper-lens and super-lens [5–9], and microsphere lens [10–18]. Among these approaches, microsphere lens assisted by a conventional optical microscope is a simple and effective method to obtain super-resolution imaging and has a promising implement in biology, medicine and other fields [13, 16]. Wang et al. [11] have demonstrated that a low-refractive-index microsphere lens with a diameter 2–9 μm can collect and magnify sub-diffraction features with a lateral resolution up to 50 nm. The microsphere lens illuminated by a standard white-light source can collect the near-field information and transfer it to the far-field propagating waves which can be picked up by a conventional optical microscope. Recently Li et al. [16] have developed the submerged microsphere optical microscopy in biology and successfully obtained direct white-light optical imaging of 75-nm adenoviruses. The optical super-resolution capability can be achieved by using a low-index microsphere semi-immersed in ethanol [17] or a high-index barium titanate glass (BTG) microsphere totally immersed in liquid or elastomers [18, 19]. The far-field imaging properties where the object is spatially separated by a SU-8 layer have also been studied [20]. The super-resolution imaging properties of the dielectric microsphere lens can be explained by the methods of “Mie scattering” [21], “whispering gallery mode” [22], “Poynting vector field” [23], or “photonic nanojets” [24–27]. The sizes of the well-studied microsphere lens as mentioned above are almost within several to several tens of microns. However, according to geometric optics, when the scale of the microsphere lens is well

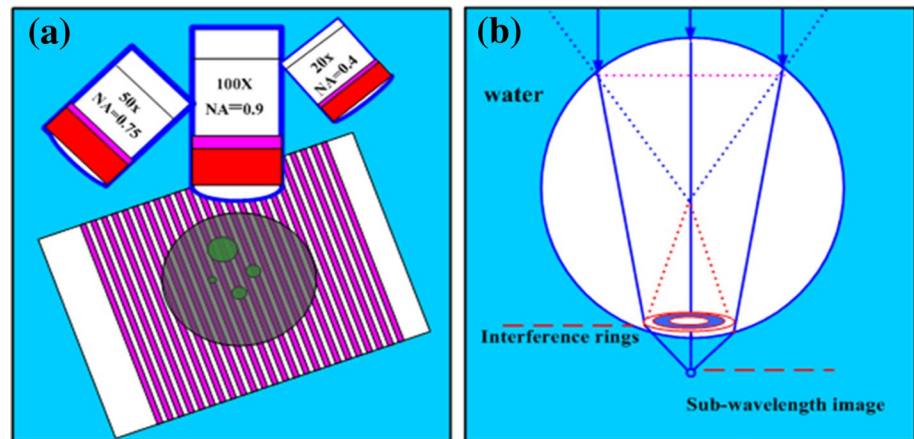
✉ Yong-Hong Ye
yeyonghong@njnu.edu.cn

Minglei Guo
Guomlnj@163.com

¹ Department of Physics, Nanjing Normal University, Nanjing 210097, China

² Department of Optoelectronic Engineering, Anhui Science and Technology University, Chuzhou 233100, China

Fig. 1 **a** Schematic of the experimental setup. **b** Imaging properties of the microsphere lens including interference rings and sub-wavelength images



larger than the optical wavelength, the image obtained by the microsphere can be explained by geometric optics [28]. Moreover, studies have shown that, when the focal plane of the objective lens is shifted, the microsphere lens can form different electric field distributions, which can result in different image properties [29]. Compared to the well-studied microsphere lens with a super-resolution capability, the imaging properties as a function of the microsphere diameter have not been studied. In this letter, we have experimentally investigated the optical imaging properties by using high-index ($n = 1.9$) BTG microsphere lenses with a diameter 5–300 μm , and the microsphere lenses are totally immersed in water ($n = 1.33$). We find that, as the focal plane of the objective lens shifts, the light beams can be concentrated by the microsphere lens to the bottom of the microsphere or form a focus with sub-wavelength waist underneath the microsphere, and thus interference rings or an optical image of the Blu-ray disk (our sample) can be seen, respectively. As the diameter of the microsphere increases, especially when it is close to the scale of geometric optics, the interference rings will increase in number and be more clear, while the resolution capability of the microsphere lens decreases as the image contrast weakens. Our simulated results indicate that the electric field distribution generated by the microsphere including the effect of “photonic nanojet” performs an important role in the imaging properties.

2 Experimental arrangement

As illustrated in Fig. 1a, a conventional microscope equipped with a CCD camera is used under a reflective illumination mode to observe our samples. Microsphere lenses with different sizes are spread on the top of the object and immersed in de-ionized water. The object sample used in the experiment is a commercial Blu-ray disk (BD) with its protection layer peeled off before use. We consider

the objective lens of the ZEISS microscope (Axio Imager A2m) combined with the microsphere lens as a unit optical system. Figure 1b illustrates that a white-light source with a peak wavelength 540 nm generated from a halogen lamp is concentrated by the microsphere lens. When the focal plane of the objective lens is shifted, different distributions of the electric field are formed, resulting in different imaging properties. First, direct image of the microsphere lens can be observed through the objective lens. Then, in the region with several microns scale near the bottom of the microsphere lens, the reflective lights generated from the lower surface of the microsphere lens and the plane of the object samples can form interference ring images, due to the superposition of the two reflective lights. Finally, when the focal plane of the objective lens is further turned down, the images of the BD sample (magnified by microsphere lens) can be formed underneath the surface of the microsphere lens, which results from the formation of a focus with sub-wavelength waist.

3 Results and discussion

Figure 2 illustrates the observed interference rings images. We can clearly see the conversion of the interference rings as the diameter of the microsphere lens increases, for the microsphere lens with a diameter of 30 μm , a central bright spot with blur surrounding rings can be formed by the microsphere lens, as shown in Fig. 2a. The surrounding rings increases in number and gradually become clear as the diameter of the microsphere increases to 60 μm (Fig. 2b). When the diameter of the microsphere lens is about 150 μm , clear interference rings which are common in conventional wave optics can be formed as shown in Fig. 2c. According to conventional wave optics, in the region near the contact point between the microsphere and the object, two planes including the low surface of the microsphere lens and the objective surface can reflect the

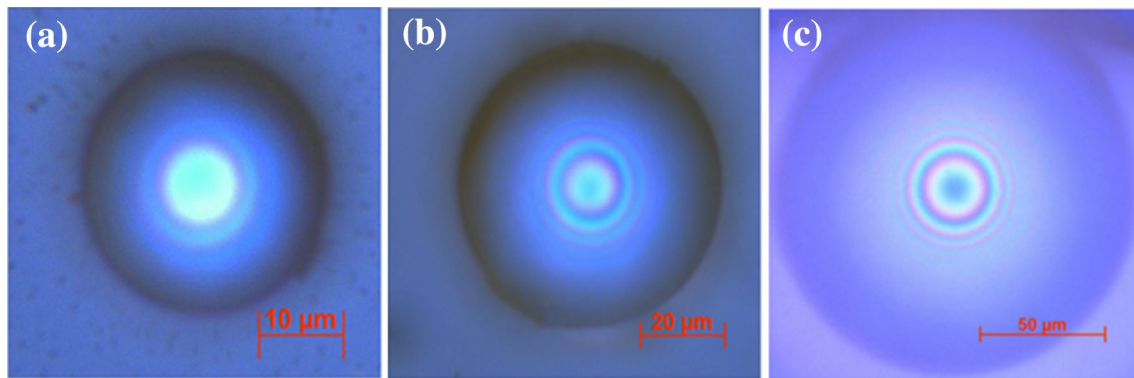
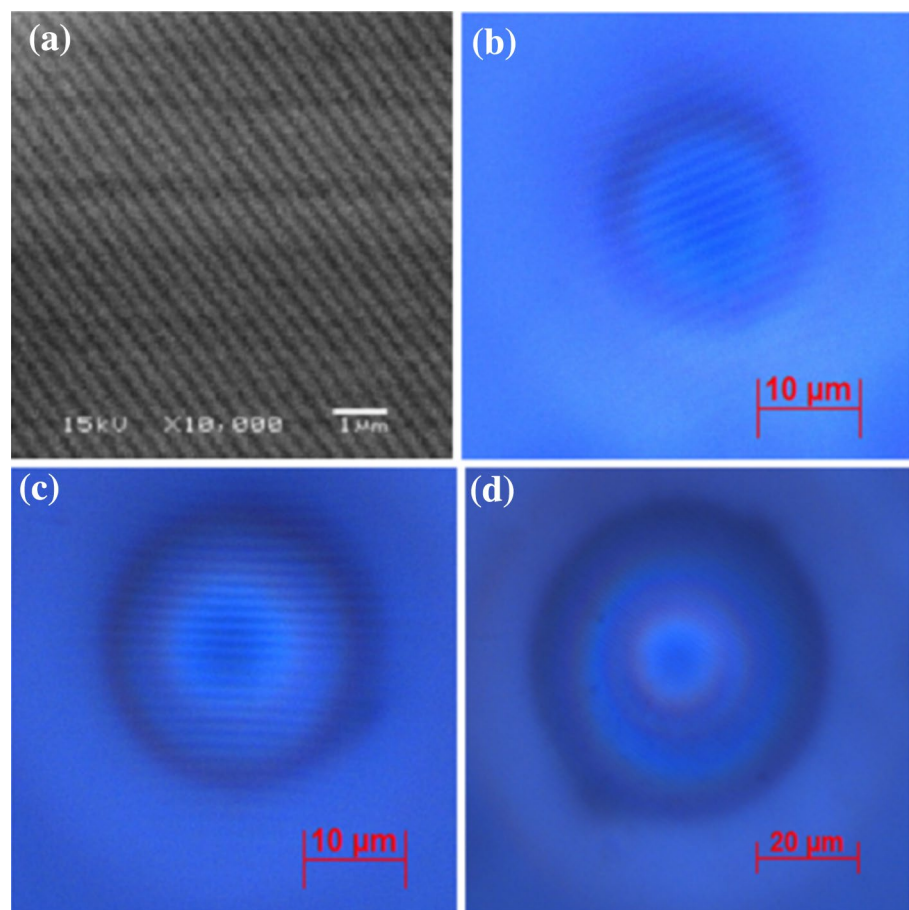


Fig. 2 Experimental interference rings formed by the microsphere lens assisted by conventional microscope. The diameter of the water-immersed microsphere lens is **a** 30 μm , **b** 60 μm , **c** 150 μm , respectively

Fig. 3 **a** SEM image of the BD sample and its sub-wavelength image using ZEISS microscope 50 \times (NA = 0.75) objective assisted by a microsphere lens immersed in water with different diameters, **b** 20 μm , **c** 30 μm , **d** 100 μm

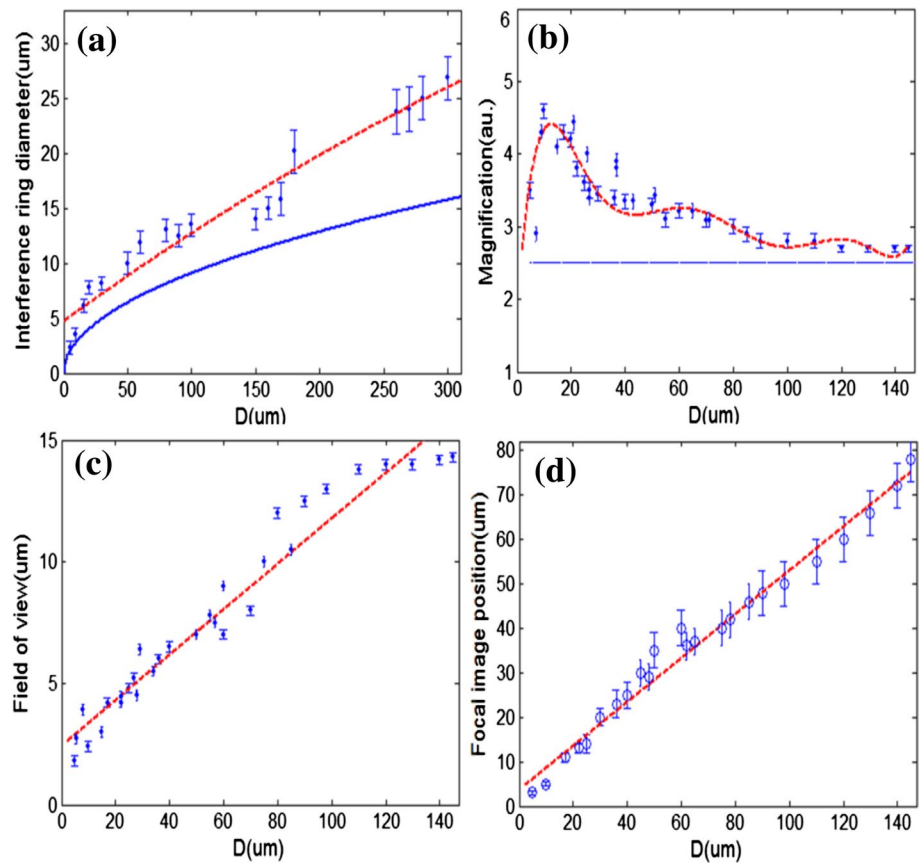


light beams from the illuminating source. The reflected lights can form interference rings due to different optical paths determined by the space between the two planes. An appropriate relation can be described as $r^2 = d \times D$, here D is the diameter of the microsphere, d is the distance between the object plane and the microsphere lens, and r is the horizontal distance from the contact point. The

interference takes place based on the condition that d is equal to $K\lambda$, here K is an integer.

Sub-wavelength images due to the microsphere focus can be formed as the focal plane of the objective lens is further turned down. The moved distance of the focal plane is only several microns. The BD sample consists of 200 nm stripes separated by 100 nm grooves, as shown in Fig. 3a

Fig. 4 **a** Diameter of the first-order interference ring as a function of the microsphere diameter for the interference rings image. (*red lines*-experimental results and *blue lines*-calculated results). **b** Magnification **c** field of view and **d** focal image position of the sub-wavelength image as a function of the microsphere diameter



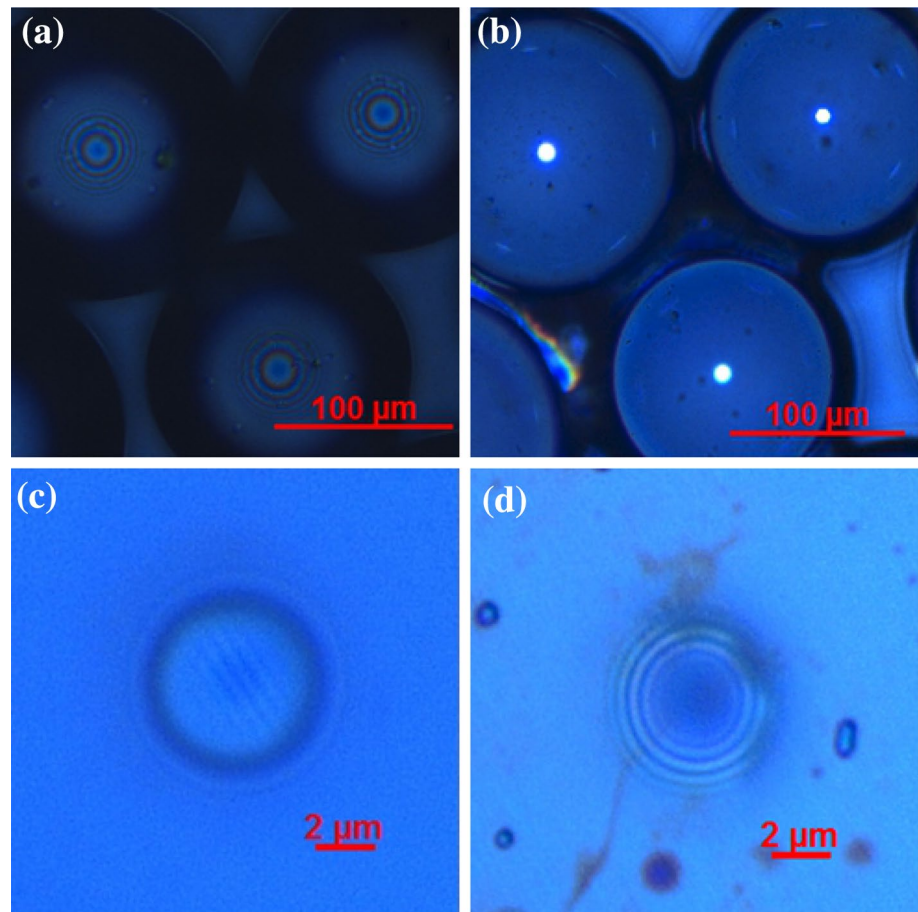
(SEM image of the BD sample), and cannot be resolved by a conventional optical microscope, while its structures can be discerned by the microsphere lens. Figure 3b shows that the microsphere lens with a diameter about $20\ \mu\text{m}$ has a high magnification which is about $4.5\times$. Microspheres with a diameter of $5\text{--}20\ \mu\text{m}$ have the best image contrast as the stripes of the BD sample can be clearly resolved. The resolution decreases as the diameter of the microsphere lens increases, which can be seen in Fig. 3c, d. When the microsphere diameter increases to $100\ \mu\text{m}$, the magnification gradually decreases to $2.8\times$, and the image contrast becomes low, as shown in Fig. 3d. When the diameter of the microsphere lens reaches up to $150\ \mu\text{m}$, the structures of the BD cannot be resolved under our experimental conditions due to the image contrast is too low.

For the interference rings, we have measured the diameter of the first-order bright interference rings. The experimental and numerical results based on the conventional wave optics are shown in Fig. 4a. For the microsphere with a diameter of $150\text{--}300\ \mu\text{m}$, which is closer to the scale of geometric optics, the diameter of first-order light ring is in the range of $15\text{--}30\ \mu\text{m}$. The experimental data are larger than the calculated value due to the magnification of the microsphere lens. For the microsphere lens with a diameter which increases from 30 to $100\ \mu\text{m}$, the experimental

value increases from 8.2 to $20.1\ \mu\text{m}$. Moreover, for the microsphere lens with a diameter less than $30\ \mu\text{m}$, only one bright ring can be formed. The diameter of the bright ring for the microsphere with a diameter of $5\ \mu\text{m}$ is only about $2.4\ \mu\text{m}$. Figure 4a shows that the tendency of the experimental results is close to the calculated values, which indicates that the interference rings can similarly be described by the conventional wave optics.

For the sub-wavelength images, the magnification calculated by geometrical optics can be estimated as $M \sim \ln / (2 - n')$ ~ 2.5 , here n' is the refractive index contrast between the BTG microsphere lens and water. The value of n' in our experiments is about 1.43 . The experimental values tend asymptotically to the geometric optics values as the diameter increases, as shown in Fig. 4b. The experimental data of the field of view (FOV) and focal image position as a function of diameter are presented in Fig. 4c, d, respectively. Here, FOV is defined as the diameter of disk area that can be discerned by the microsphere [30]. Compared to the low-index microsphere lens, the FOV of the BTG microsphere can be spread to a large region due to its high index [18]. The FOV is another important property of the microsphere lens. As the microsphere diameter increases from 5 to $100\ \mu\text{m}$, the FOV increases from 1.8 to about $14\ \mu\text{m}$, as shown in Fig. 4c. Figure 4d shows the

Fig. 5 Images obtained by the microsphere lens with diameter **a** 180 μm fully immersed in water, **b** 180 μm in air, **c** 5 μm fully immersed in water, **d** 5 μm in air



virtual focal image position (FIP) below the object surface plane for microsphere lenses with different diameters, and the experimental results demonstrate that the focal image position increases as a function of diameter, which can reach up to about 50 μm , which means that sub-wavelength imaging of BTG microsphere lens can be formed at a large distance. It should be noted that the imaging magnification and contrast will be greatly affected by the focal image position.

Our experiments also show that the surrounding medium has a great effect on imaging properties of the microsphere lens. For the microsphere with a diameter $\sim 180 \mu\text{m}$ fully immersed in the medium, the clear interference rings can be captured, but the interference rings will disappear when the medium almost evaporates. The diameter of the interference ring gradually reduces, and the intensity of the interference ring gradually weakens as the liquid slowly evaporates. The process is exhibited in Fig. 5a, b. For the microsphere lens with a diameter $\sim 5 \mu\text{m}$, it can discern the sub-wavelength patterns of the BD sample when it is absolutely immersed in water. As shown in Fig. 5c, stripes of the BD samples can be seen clearly through the microsphere lens with a magnification about $3.5 \times$. But when water disappears, the image of the

BD will be lost, as shown in Fig. 5d. The important role of the immersed medium can be expected, as the electric field distribution of the microsphere lens is greatly affected by the refractive index contrast and the immersed medium allows the sub-wavelength focus to be produced outside of microsphere [24].

In order to give a reasonable explanation to our studies, finite-difference time-domain simulation is carried out to calculate the electric field distribution. The rightward-propagating incident light has a wavelength of 540 nm in our calculations. The transverse-field profiles are drawn based on the light intensity. Figure 6 presents the calculated transverse field distributions when the objective lens shifts on different cross sections of the microsphere lens with a diameter 30 μm . As shown in Fig. 6a, interference rings can be formed at the plane above the bottom of the microsphere (about 4.9 μm), and the light beams can be further compressed which is shown in Fig. 6b, when the focal plane of the objective lens is tuned down, which is about 2.1 μm above the bottom of the microsphere. The interference rings stem from the interference of the reflective light beams as described in the conventional physics optics. The concentric rings can form far-field sub-wavelength focusing, which has been experimentally verified [31].

Fig. 6 Evolution of the electric field distribution as the z-position along the incident axis shifts. **a** interference rings, **b** interference rings with further compression **c** sub-wavelength focus **d** sub-wavelength focus with diffuseness. The *curves* below them are the transverse electric field profiles. The diameter of the microsphere is $30\ \mu\text{m}$ and the wavelength of the incident light is $540\ \text{nm}$

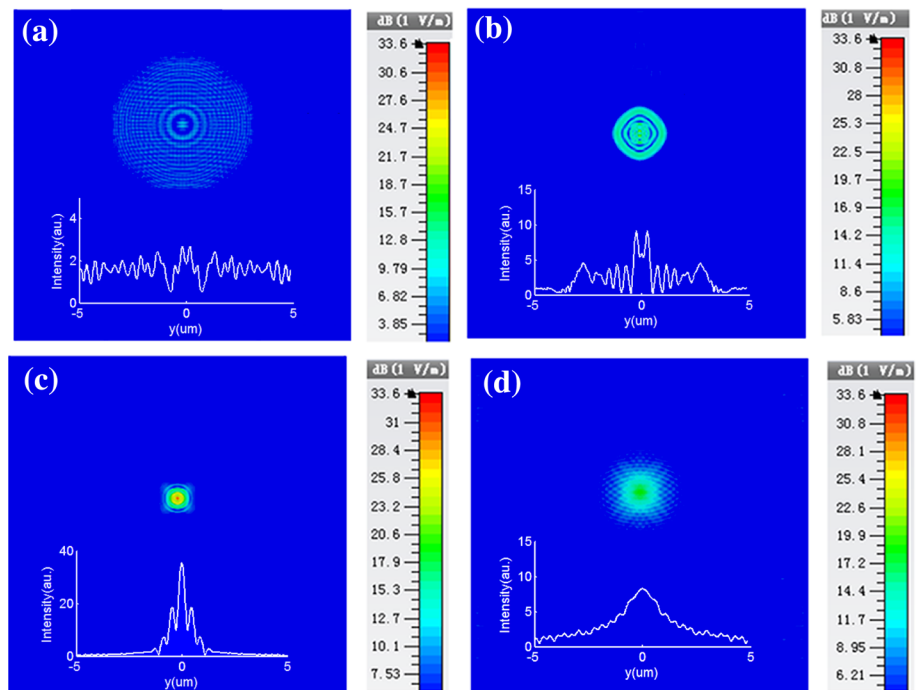
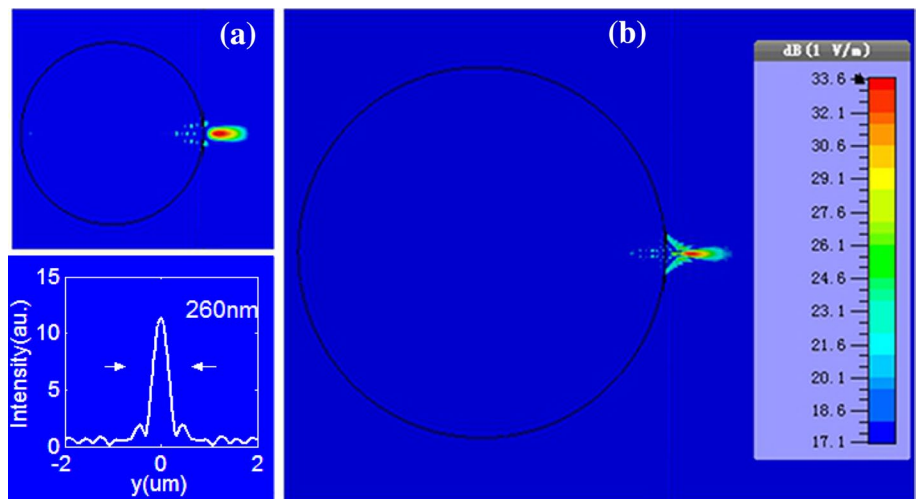


Fig. 7 **a** Electric field intensity distribution and the FWHM ($260\ \text{nm}$) of the “photonic nanojet” formed by microsphere lens with diameter $5\ \mu\text{m}$ **b** Electron field intensity distribution of the microsphere lens with diameter $30\ \mu\text{m}$. The results are simulated by CST



According to our calculated results, the sub-wavelength focus is generated at the plane below the microsphere at about $1.6\ \mu\text{m}$, as shown in Fig. 6c. Figure 6d illustrates that the focus will diffuse as the focal plane moves away from the microsphere lens. Moreover, as the diameter of the microsphere increases, the interference rings become more clear with the increase in the diameter of the center spot and the number of the ring, which are consist with our experiment results (Figs. 2, 4a). The increase in the diameter of the rings indicates the loss of the diffraction light intensity in the far field, which is similar to the mechanism of the grating diffraction, and this will result in the

reduction in the sub-wavelength focusing capability of the microsphere lens.

The focus in the shadow of the microsphere has a strong electric field termed as “photonic nanojet”, which means the specific spatial region within the external focal waist of the light wave diffracted on microspheres or microcylinders [24]. The nanojet which can induce strong background scattering indicates that super-resolution imaging can be formed, and the background scatter effect of the photonic nanojet is experimentally verified [26, 27]. The sub-wavelength imaging capability in our experiment can be related to the full width at half maximum (FWHM) of

the photonic nanojets. Figure 7a shows that, for the microsphere with a diameter of 5 μm , the FWHM of the nanojets is about 260 nm. The half-wavelength scale of the nanojet waist indicates a high-quality sub-wavelength imaging can be achieved. For microsphere lenses with a diameter of 30 μm (as shown in Fig. 7b) and 50 μm , the FWHM of the nanojets is 320 nm and 380 nm, respectively. The position of the maximum electric intensity is about $0.1 R \sim 0.18 R$ under the low surface of the microsphere lens, where R is the radius of microsphere lens. When the microsphere diameter increases, the waist of the photonic nanojet broadens and focus capability weakens. Moreover, a large microsphere diameter means long propagating distance, which induces heavy loss of the evanescent waves that carry sub-wavelength imaging information. Therefore, the resolution of the microsphere reduces as the microsphere diameter increases, and only conventional interference rings can be formed when the microsphere diameter is larger than 150 μm in our experiments, although it might also have sub-wavelength imaging capability under other microscopes such as a confocal microscopic system. It should be emphasized that, besides the nanojet effect discussed in this paper, some other mechanisms must contribute to the microsphere imaging, such as surface wave or quantum effects.

4 Conclusions

In conclusion, we have observed the conversion of imaging properties of high-index microsphere lenses as a function of the microsphere diameter. Our experiments demonstrate that interference rings and sub-wavelength images can be observed through the microsphere lens by adjusting the focal plane of the objective lens. Both the two properties are dependent on the microsphere diameter. The immersion medium is important for the forming of both the sub-wavelength images and the interference rings. The electric field distribution of the microsphere and the FWHM of the “photonic nanojets” in the shadow of the microsphere lens can be used to explain the imaging properties.

Acknowledgments This research was supported by Doctoral Fund of Ministry of Education of China (No. 20133207110007) and National Nature Science Foundation of China (Grant No. 61475073).

References

1. X. Zhang, Z. Liu, *Nat. Mater.* **7**, 435 (2008)
2. S. Kawata, Y. Inouye, P. Verma, *Nat. Photonics* **3**, 388 (2009)
3. S.W. Hell, J. Wichmann, *Opt. Lett.* **19**, 780 (1994)
4. B. Hecht, B. Sick, U.P. Wild, V. Deckert, R. Zenobi, O.J.F. Martin, D.W. Pohl, *J. Chem. Phys.* **112**, 7761 (2000)
5. S.W. Hell, R. Schmidt, A. Egner, *Nat. Photon* **3**, 381 (2009)
6. E.G. van Putten, D. Akbulut, J. Bertolotti, W.L. Vos, A. Lagendijk, A.P. Mosk, *Phys. Rev. Lett.* **106**, 193905 (2011)
7. J. Rho, Z. Ye, Y. Xiong, X. Yin, Z. Liu, H. Choi, G. Bartal, X. Zhang, *Nat. Commun.* **1**, 1148 (2010)
8. E. Rogers, J. Lindberg, T. Roy, S. Savo, J.E. Chad, M.R. Dennis, N.I. Zheludev, *Nat. Mater.* **11**, 432 (2012)
9. F. Lemoult, M. Fink, G. Lerosey, *Nat. Commun.* **3**, 889 (2012)
10. J.Y. Lee, B.H. Hong, W.Y. Kim, S.K. Min, Y. Kim, M.V. Jouravlev, R. Bose, K.S. Kim, I.C. Hwang, L.J. Kaufman, C.W. Wong, P. Kim, K.S. Kim, *Nature* **460**, 498 (2009)
11. Z. Wang, W. Guo, L. Li, B. Luk'yanchuk, A. Khan, Z. Liu, Z. Chen, M. Hong, *Nat. Commun.* **2**, 218 (2011)
12. D.A. Fletcher, K.B. Crozier, C.F. Quate, G.S. Kino, K.E. Goodson, D. Simanovskii, D.V. Palanker, *Appl. Phys. Lett.* **77**, 2109 (2000)
13. H. Yang, N. Moullan, J. Auwerx, M.A. Gijs, *Small* **10**, 1712 (2014)
14. Y. Duan, G. Barbastathis, B. Zhang, *Opt. Lett.* **38**, 2988 (2013)
15. D.A. Fletcher, K.E. Goodson, G.S. Kino, *Opt. Lett.* **26**, 399 (2001)
16. L. Lin, W. Guo, Y. Yan, S. Lee, T. Wang, *Light Sci. Appl* **2**, e104 (2013)
17. X. Hao, C. Kuang, X. Liu, H. Zhang, Y. Li, *Appl. Phys. Lett.* **99**, 203102 (2011)
18. A. Darafsheh, G.F. Walsh, L.D. Negro, V.N. Astratov, *Appl. Phys. Lett.* **101**, 141128 (2012)
19. A. Darafsheh, C. Guardiola, A. Palovcak, J.C. Finlay, A. Cárabe, *Opt. Lett.* **40**, 010005 (2015)
20. R. Ye, Y. Ye, H.F. Ma, J. Ma, B. Wang, J. Yao, S. Liu, L. Cao, H. Xu, J. Zhang, *Opt. Lett.* **38**, 1829 (2013)
21. A.D. Kiselev, D.O. Plutenko, *Phys. Rev. A* **89**, 043803 (2014)
22. Y. Yan, Y. Zeng, Y. Wu, Y. Zhao, L. Ji, Y. Jiang, L. Li, *Opt. Express* **25**, 23552 (2014)
23. S. Lee, L. Li, Z. Wang, *J. Opt.* **16**, 015704 (2014)
24. Z. Chen, A. Taflove, V. Backman, *Opt. Express* **12**, 1214 (2004)
25. X. Li, Z. Chen, A. Taflove, V. Backman, *Opt. Express* **13**, 526 (2005)
26. A. Heifetz, K. Huang, A.V. Sahakian, X. Li, A. Taflove, V. Backman, *Appl. Phys. Lett.* **89**, 221118 (2006)
27. S. Yang, A. Taflove, V. Backman, *Opt. Express* **19**, 7084 (2011)
28. M. Sasaki, T. Kurosawa, K. Hane, *Appl. Phys. Lett.* **70**, 785 (1997)
29. D.R. Mason, M.V. Jouravlev, K.S. Kim, *Opt. Lett.* **35**, 2007 (2010)
30. V. Pacheco-Peña, M. Beruete, I.V. Minin, O.V. Minin, *Appl. Phys. Lett.* **105**, 084102 (2014)
31. T. Wang, X. Wang, C. Kuang, X. Hao, X. Liu, *Appl. Phys. Lett.* **97**, 231105 (2010)